ELSEVIER

Contents lists available at ScienceDirect

Science of the Total Environment

journal homepage: www.elsevier.com/locate/scitotenv





Assess the formation of disinfection by-products from pyrogenic dissolved organic matter (pyDOM): impact of wildfire on the water quality of forest watershed

Zhao Li ^a, Pamela Rose V. Samonte ^a, Han Cao ^a, Jessica R. Miesel ^b, Wenqing Xu ^{a,*}

- a Department of Civil and Environmental Engineering, Villanova University, 800 E. Lancaster Ave., Villanova, PA 19085, United States of America
- b Department of Plant, Soil and Microbial Sciences, Michigan State University, 220 Trowbridge Rd, East Lansing, MI 48824, United States of America

ARTICLE INFO

Editor: Jay Gan

Keywords:
Nitrosamines
Haloacetic acids
Trihalomethanes
Electrochemical reduction
Electron-exchange capacity
Chlorination
Chloramination

ABSTRACT

Wildfires can release pyrogenic dissolved organic matter (pyDOM) into the forest watershed, which may pose challenges for water treatment operations downstream due to the formation of disinfection by-products (DBPs). In this study, we systematically assessed the physio-chemical properties of pyDOM (e.g., electron-donating and -accepting capacities; EDC and EAC) and their contributions to DBP formation under different disinfection scenarios using (1) ten lab samples produced from various feedstocks and pyrolysis temperatures, and (2) preand post-fire field samples with different burning severities. A comprehensive suite of DBPs-four trihalomethanes (THMs), nine haloacetic acids (HAAs), and seven N-nitrosamines—were included. The formations of THM and HAA showed an up to 5.7- and 8.9-fold decrease as the pyrolysis temperature increased, while the formation of N-nitrosamines exhibited an up to 6.6-fold increase for the laboratory-derived pyDOM. These results were supported by field pyDOM samples, where the post-fire samples consistently showed a higher level of Nnitrosamine formation (i.e., up to 5.3-fold), but lower THMs and HAAs compared to the pre-fire samples. To mimic environmental reducing conditions, two field samples were further reduced electrochemically and compared with Suwannee River natural organic matter (SRNOM) to evaluate their DBP formation. We found increased DBP formation in pyDOM samples following electrochemical reduction but not for SRNOM, which showed increased N-nitrosamines but decreased THMs and HAAs post-electrochemical reduction. Furthermore, this study reported for the first time the formation of two previously overlooked N-nitrosamines (i.e., nitrosodiethylamine (NDEA), N-nitrosodi-n-propylamine (NDPA)) in both laboratory and field pyDOM samples, raising concerns for drinking water safety given their higher toxicity as compared to the regulated counterparts. Results from this study provide new insights for DBP mitigation during post-fire recovery, which are particularly relevant to communities that rely on forest watersheds as their drinking water sources.

1. Introduction

The provision of access to clean water is one of the grand challenges identified by the National Academy of Engineering (NAE, 2019). Approximately one-third of the United States population receives drinking water from forest watersheds (Wang et al., 2015b). Yet, these water sources are increasingly threatened by wildfires (Cannon and DeGraff, 2009; Smith et al., 2011). With the changing climate and increased human activities in the forest environment, the frequency, extent, and severity of wildfires have skyrocketed globally—a trend predicted to continue (Bladon et al., 2014; Hohner et al., 2019; Rhoades et al., 2019). In addition to consuming significant amounts of forest

biomass, wildfires also transform a portion of biomass into pyrogenic organic matter (pyOM; e.g., char) (Maestrini et al., 2017; Miesel et al., 2018), subsequently altering dissolved organic matter (DOM) exported to forest watersheds, which may adversely impact downstream water quality (Hohner et al., 2019; Wang et al., 2015a). In particular, chars from wildfires could release a heterogeneous mixture of diverse (macro) molecules into the aquatic environment, hereinafter referred to as pyrogenic dissolved organic matter (pyDOM; operationally defined as the fraction of organic carbon that passes through 0.45 μ m filters) (Abiven et al., 2011; Fu et al., 2016; Liu et al., 2019; Song et al., 2021; Sun et al., 2021; Zheng et al., 2023; Wang et al., 2021; Xu et al., 2021; Zhang et al.,

E-mail address: wenqing.xu@villanova.edu (W. Xu).

^{*} Corresponding author.

2019; Zheng et al., 2019), containing more oxygen content and polar functional groups but lower aromaticity than its respective bulk chars (Qu et al., 2016). As a result, pyDOM is relatively mobile and can be transported across long distances (Major et al., 2010), contributing to the increased dissolved organic carbon (DOC) and nitrogen (DON) in forest watersheds following wildfires (Emelko et al., 2011; Jaffé et al., 2013).

DOC and DON have long been recognized as precursors for disinfection by-products (DBPs), which are a suite of toxic chemicals formed from the reaction of chlorine or chloramine with organic precursors in the water during disinfection (Krasner, 2009; Mitch, 2009; USEPA, 2006). Mounting epidemiological and lab toxicology evidence suggest potential human health concerns associated with DBPs, such as bladder cancer and reproductive and developmental effects (Muellner et al., 2007; Richardson et al., 2007; Richardson and Ternes, 2014), As such, certain carbon-based DBPs, such as trihalomethanes (THMs) and haloacetic acids (HAAs), are regulated at 80 μ g L⁻¹ and 60 μ g L⁻¹, respectively, by the United States Environmental Protection Agency (USEPA) under Stage 1 and 2 of the Disinfectants and Disinfection By-Products Rules (DeMarini, 2020; Pals et al., 2011; Pandian et al., 2022; USEPA, 2006). However, in vitro mammalian cell tests have indicated that many unregulated nitrogen-based DBPs, such as N-nitrosamines (e.g., Nnitrosodimethylamine (NDMA)), haloacetonitriles (HANs), and halonitromethanes (HNMs), show higher cyto- and geno-toxicity than their regulated counterparts (e.g., THM and HAA), observed by the lower LC_{50} with nitrogen-based DBPs (i.e., $10^{-5.7}$ with dibromoacetonitrile) than carbon-based DBPs (i.e., $10^{-5.05}$ with monobromoacetic acid) (Bond et al., 2012; Bond et al., 2011; Plewa et al., 2008; Richardson et al., 2007; USEPA, 2006).

Previous studies using pyDOM extracted from chars prepared under well-controlled laboratory conditions observed lower HAA and THM formation with increasing pyrolysis temperature (Chen et al., 2022; Li et al., 2022; Yang et al., 2022). By contrast, studies with field samples collected from the same locations pre- and post-fire have reported conflicted results with respect to the DBP formation (i.e., such as NDMA (Olivares et al., 2021; Wang et al., 2016; Wang et al., 2015b), HAAs (Wang et al., 2016; Writer et al., 2014), and THMs (Hohner et al., 2016; Revchuk and Suffet, 2014; Wang et al., 2016)), possibly due to the complexity of field conditions. Thus, there is a need to reconciliate studies from well-controlled laboratory conditions and field work to guide future efforts in post-fire recovery and DBP mitigation. Moreover, previous studies only investigated pyDOM from limited char specimens under either chlorination or chloramination (Chen et al., 2022; Chen et al., 2021; Li et al., 2022; Wang et al., 2023; Yang et al., 2022). Most existing work focused on HAAs and THMs, whereas information on Nnitrosamines is scarce except for NDMA (Hohner et al., 2016; Lee et al., 2022; Li et al., 2022; Revchuk and Suffet, 2014; Wang et al., 2015a; Wang et al., 2016; Writer et al., 2014; Yang et al., 2022). Furthermore, the redox properties of pyDOM may be altered by the reducing or oxidizing conditions upon their entrance or further transport in the environment (e.g., serve as an electron acceptor for microbial respiration) (Klüpfel et al., 2014; Sun et al., 2021), which may subsequently impact the formation of DBPs when the water is sourced for drinking water. However, no knowledge is available on this topic.

This study aims to systematically investigate the contribution of pyDOM specimens to DBP formation under different disinfection scenarios through the analysis of a comprehensive suite of DBPs with pyDOM samples from laboratory-prepared samples and field samples. Specifically, we extracted pyDOM from (1) ten laboratory-produced chars pyrolyzed from two feedstocks (oak wood (*Quercus robur*) and switchgrass (*Panicum vigartum*)) at five different temperatures (300, 400, 500, 600, and 700 °C) and (2) pre- and post-fire field samples collected from active wildfire incidents in mixed-conifer forests in California, USA characterized by varying burn severities (i.e., low and high severities) (Miesel et al., 2018). We then assessed the physio-chemical properties of pyDOM by characterizing the non-purgeable organic

carbon (NPOC), total nitrogen (TN), specific ultraviolet absorbance at 254 nm (SUVA₂₅₄), E₂/E₃ values, and electron-donating (EDC) and -accepting (EAC) capacities. Afterwards, their contributions to the formation of a suite of regulated and emerging DBPs — specifically for four THMs (trichloromethane (TCM), bromodichloromethane (BDCM), dibromomethane (DBCM), tribromomethane (TBM)), nine HAAs (chloroacetic acid (MCAA), bromoacetic acid (MBAA), dichloroacetic acid (DCAA), trichloroacetic acid (TCAA), bromochloroacetic acid (BCAA), dibromoacetic acid (DBAA), bromodichloroacetic (BDCAA), chlorodibromoacetic acid (CDBAA), tribromoacetic acid (TBAA)), and seven nitrosamines (N-nitrosodimethylamine (NDMA), Nmethylethanolamine (NMEA), N-nitrosodiethylamine (NDEA), 2-nitrodiphenylamine (NDPA), N-nitrosopyrrolidine (NPYR), N-nitrosopiperidine (NPIP), *N*-nitrosodibutylamine (NDBA)) investigated. Lastly, two selected field samples and Suwannee River natural organic matter (SRNOM; reference DOM) were electrochemically reduced to mimic environmental reducing conditions, from which their impacts on DBP formation were subsequently quantified. The results from this study aim to reconcile differences between laboratory and field data and ultimately use the information to provide guidance for post-fire recovery and DBP mitigation.

2. Materials and methods

2.1. Chemicals

Fisher Scientific (Pittsburg, PA): sodium hydroxide (97.9+ %), methyl tert-butyl ether (MTBE, HPLC Grade); Sigma-Aldrich (Milwaukee, MI): dichloromethane (HPLC Grade), methanol (HPLC Grade), sodium hypochlorite (10-15 % NaOCl, reagent grade), 1,2,3trichloropropane (99 + %), sodium dihydrogen phosphate (99.0+ %), sodium sulfate (99.0+ %), 2,2-azino-bis-(3-ethylbenzthiazoline-6-sulfonic acid) diammonium salt (ABTS, 98.0+ %), diquat dibromide monohydrate (DQ, 98.0+ %), antraquinone-2, 6-disulfonate (AQDS, 90.0+ %), 1,2-dibromopropane (97+ %), deuterated *N*-nitrosodimethylamine (98+ %), disodium ethylenediamine tetraacetate dihydrate (EDTA) (97+ % crystalline), EPA 521 nitrosamine calibration mix (in methylene chloride), EPA 552 haloacetic acids mix (in MTBE), and EPA 501/601 trihalomethanes calibration mix (in methanol); BeanTown Chemical (Hudson, NH): N,N-diethyl-p-phenylenediamine (DPD) (97+ %): Suwannee River natural organic matter (SRNOM: Catalog No.: 1R101N) was purchased from the International Humic Substances Society (IHSS, St. Paul, MN); and VWR (Radnor, PA): L-ascorbic acid (99.0+ %), disodium hydrogen phosphate anhydrous (99.0+ %) were used as received. Chlorine standard solution (64.3 \pm 0.3 mg L^{-1} as Cl₂) was purchased from Hach Sigma (Loveland, CO) as a blind standard. Deionized water (18.2 M Ω cm⁻¹) was produced by a Millipore milli-Q plus water purification system.

2.2. Preparation of pyDOM

Laboratory-produced chars were prepared following the same protocol established in our previous study with minor changes (Xu et al., 2021). Briefly, the pyrolysis of oak wood (*Quercus robur*) or switchgrass (*Panicum vigartum*) was performed with a model 1600 serial CM tube furnace (CM Inc., Bloomfield, NJ) under a steady flow of N₂ (50 mL min $^{-1}$) at various temperatures (300, 400, 500, 600, and 700 °C) for 2 h. Oak wood and switchgrass depict the representative biomass composition of the forest floor layer (Reich et al., 2001; Santín et al., 2017). Herein, the obtained chars are abbreviated as WX and GX — W stands for the wood feedstock, G is the grass feedstock, and X is the pyrolysis temperature (°C). Subsequently, the chars were ground and passed through a 70-mesh sieve (ASTM Standard Test Sieve, E-11 Specification). Elemental analysis of these chars was performed by Galbraith Laboratories (PerkinElmer 2400 CHNS/O Series II; Thermo Scientific FlashEA 1112). The key properties of these chars are provided in

Table S1. To obtain the pyDOM samples, each laboratory char (20 g L $^{-1}$) was equilibrated with phosphate buffer (10 mM, pH = 7.0 \pm 0.2) on a rotator (30 rpm, in darkness, 25 °C) for 72 h, after which all samples were centrifuged at 3000g for 10 min. The supernatants were subsequently filtered through 0.45 μm PTFE membranes (VWR, USA) to obtain the pyDOM specimens. All pyDOM samples were abbreviated as pyDOM $_{WX}$ or pyDOM $_{GX}$.

Field samples were collected in a mixed-conifer forest in California, USA with assistance from the USDA Forest Service Fire Behavior Assessment Team (https://www.frames.gov/fbat/home) five days before fire and three days after fire for the low-severity samples (Pre_6 and Post_6), and approximately seven days before fire and three days after fire for the high-severity samples (Pre_10 and Post_10). Details of dates and time of the field sampling are provided in the SI (Table S8). The field sites were located in the August 2015 Rough wildfire (latitude 36.874° N, longitude 118.905° W), in areas classified as "high" or "low" burn severity as determined from post-fire field observations (Miesel et al., 2018) and remote sensing data (Eidenshink et al., 2007). The prefire field samples (Pre 6, Pre 10) consisted of the entire forest floor horizon (i.e., soil organic horizon, inclusive of litter, fermentation, and humic layers); the post-fire samples consisted of the fire-altered forest floor horizon (i.e., a mixture of ash and char derived from the soil organic horizon). The post-fire samples (Post_6, Post_10) were each collected within 1.0 m from their analogous pre-fire samples. No rainfall occurred between the pre- and post-fire sampling dates. The samples were returned to the laboratory where they were air-dried to constant mass, then milled to pass an 80-mesh screen. The physiochemical properties of field samples are provided in Table S9. All six field samples (Pre_6, Post_6, RPost_6, Pre_10, Post_10, Rpost_10) were then analyzed identically as the laboratory chars. SRNOM was also included for comparison purposes.

2.3. Characterization of pyDOM

The non-purgeable organic carbon (NPOC) and the total nitrogen (TN) of all pyDOM specimens were quantified using a total organic carbon analyzer (TOC-L, Shimadzu, Japan). The concentrations of iron (Fe) and manganese (Mn) in the laboratory-derived pyDOM samples were measured using inductively coupled plasma mass spectrometry (ICP-MS, Agilent 7900 ICP-MS, USA). The ultraviolet (UV) absorption of pyDOM was measured from a wavelength range of 200 nm to 800 nm using a UV–vis spectrophotometer (DR6000, HACH, USA). The specific ultraviolet absorbance at 254 nm (SUVA $_{254}$; L mg $_{\rm C}^{-1}$ m $^{-1}$) was calculated using Eq. (1) below, where A $_{254}$ is the ultraviolet absorbance at 254 nm (cm $^{-1}$) and C $_{\rm NPOC}$ is the non-purgeable organic carbon content (mg L $^{-1}$).

$$SUVA_{254}(L \cdot mg^{-1} \cdot m^{-1}) = \frac{A_{254}(cm^{-1})}{C_{NPOC}(mg \cdot L^{-1})} *100 (cm \cdot m^{-1})$$
(1)

The absorbance ratios at 254 nm over 365 nm were also calculated (i. e., E_2/E_3) as an approximate of the average molecular size for the pyDOM and SRNOM samples.

2.4. Electrochemical experiment

All electrochemical measurements were conducted in a glovebox (5 % $\rm H_2$, 20 % $\rm CO_2$, 75 % $\rm N_2$, $\rm O_2$ < 5 ppm, Coy Laboratory Product, Inc.). Experiments were carried out in a 25 mL glassy carbon working electrode cylinder (Sigradur G, HTW, Germany) with an Ag/AgCl reference electrode (Bioanalytical Systems, Inc., West Lafayette, IN) and a counter electrode of a coiled platinum wire (Bioanalytical Systems, Inc., West Lafayette, IN) in a compartment separated from the glassy carbon by a porous glass frit. A magnetic stir bar was used to ensure proper mixing during the EDC and EAC measurements. A CH Instruments 630C electrochemical station (Austin, TX) was used to measure the currents $\it I$ (A) and control potentials.

2.4.1. EDC and EAC analysis of pyDOM specimens

Two setups were used for EDC and EAC quantifications, respectively, following previously established protocols (Aeschbacher et al., 2010; Walpen et al., 2018; Xu et al., 2021). In brief, 20 mL of buffer (0.1 M KCl, 0.1 M phosphate, pH 7) was added to the glassy carbon cylinder, where fixed potentials were applied for EDC ($E_h = +0.61$ V vs. standard hydrogen electrode (SHE)) and EAC ($E_h = -0.49\ V$ vs. SHE), respectively (Aeschbacher et al., 2012b). To generate the oxidative or reductive current peaks, 5 mL of the electron transfer mediators (1 mM ABTS or DQ²⁺) was introduced into the cylinder. Once the redox equilibrium between ABTS/ABTS⁺⁺ or DQ²⁺/DQ⁺⁺ was obtained at the working electrode (the current returned to a background level of $\sim 10^{-6}$ A), 100 μL of pyDOM (in duplicate) was added to generate the quantifiable current peaks. The EDC and EAC values were calculated by integrating the oxidative current peak (ABTS to ABTS.*) and the reductive current peak (DQ²⁺ to DQ•⁺) over time, respectively, which were further converted to the number of electrons transferred from or to the injected sample through calibration with redox standards. Calibration curves were constructed using ascorbic acid and AQDS as standards for EDC and EAC, respectively. Additionally, their relative contributions of two major redox-active metals in pyDOM samples (i.e., Fe and Mn) to electron-exchange capacity (EEC) were calculated, where we assumed the exchange of 1 mol e⁻ per mole Fe and Mn (i.e., redox couple Fe³⁺/ Fe^{2+} , and Mn^{4+}/Mn^{3+} or Mn^{3+}/Mn^{2+}) (Xu et al., 2021).

2.4.2. Electrochemical reduction of pyDOM

To electrochemically reduce pyDOM, the same three-electrode setup (described in Section 2.4.1) was used in the absence of electron transfer mediators. Two pyDOM from the field sites (post-fire samples from each low- and high-severity site) were included, where the electrochemically reduced samples from the low- and high-severity burn sites were abbreviated as Rpost_6 and Rpost_10, respectively. SRNOM was also reduced for comparison purposes, hereafter abbreviated as RSRNOM. The pre-reduced samples were transferred directly to the glassy carbon cylinder without further dilution; their NPOC values are reported in Table S3. A reduction potential of -0.47 V (vs. SHE) was applied to initiate electrochemical reduction following previous established protocols (Walpen et al., 2016). The reductive current was continuously monitored and the experiment was terminated after 24 h when the reductive current returned to the background level ($\sim 10^{-6}$ A). All the experiments were conducted in duplicate.

2.5. Disinfection experiments

A NaOCl stock solution (0.03 mM) was prepared by diluting sodium hypochlorite (15 wt%) in DI water, which was subsequently standardized on an ultraviolet-visible (UV–vis) spectrophotometer at the wavelength of 292 nm (Furman and Margerum, 1998; Schreiber and Mitch, 2005). NH₂Cl was prepared by adding 5 mL of NaOCl (0.03 mM) into 5 mL of NH₄Cl (0.036 mM, pH = 8.5 ± 0.1) drop-by-drop to achieve a Cl/N molar ratio of at least 1:1.2 (Furman and Margerum, 1998; Schreiber and Mitch, 2005). The obtained solution was standardized using UV–vis spectrophotometry at 245 nm and 295 nm for NH₂Cl and NHCl₂, respectively (Furman and Margerum, 1998; Schreiber and Mitch, 2005).

All disinfection experiments were performed in 40 mL borosilicate glass bottles with Teflon lined caps under a headspace-free condition at room temperature (25 \pm 1 $^{\circ}$ C) in the dark. Blank controls without pyDOM and SRNOM were simultaneously prepared. All pyDOM samples were first diluted with 10 mM phosphate buffer to achieve an initial concentration of 3 mg $_{\rm C}$ L $^{-1}$ at pH 8.0 \pm 0.1 prior to disinfection. Subsequently, a dose of 4.5 mg L $^{-1}$ (as Cl $_{\rm 2}$) of disinfectant was added in the form of NaOCl (chlorination) or NH $_{\rm 2}$ Cl (chloramination) (Li et al., 2017; USEPA, 2023) with the aim of maintaining a chlorine residual of 1–2 mg L $^{-1}$ after 3 d of disinfection at 25 $^{\circ}$ C (Table S3). After 72 h, samples were quenched by adding 70 mM ascorbic acid and analyzed for residual chlorine and DBPs. The residual chlorine concentrations were measured

using the *N*,*N*-diethyl-*p*-phenylenediamine (DPD) colorimetric method (Association et al., 1915).

2.6. Disinfection by-product (DBP) analysis

The quantification of the DBPs was performed following previously established protocols (Li et al., 2017; Samonte et al., 2022). Trihalomethane (THM) analysis was completed following a method adapted from EPA method 551.1 (USEPA, 1995). In brief, the aqueous phase was first pipetted out. Liquid-liquid microextraction was then carried out with methyl tert-butyl ether (MTBE; with 200 μ g L⁻¹ 1,2-dibromopropane as internal standard) at a 1:1 volumetric ratio, followed by 3-min vortexing. Conversely, N-nitrosamine quantification followed a method adapted from EPA method 521 (USEPA, 2004), wherein dichloromethane (DCM; with 100 ng L⁻¹ N-nitrosodimethylamine-d6 as internal standard) was added to the water samples at a 1:5 volumetric ratio, followed by 5-min vortexing. Afterwards, approximately 3 mL of DCM extracts were collected, concentrated, and reconstituted to 200 μ L. Both THMs and N-nitrosamines were analyzed by gas chromatography coupled with mass spectrometry (GC/MS; Agilent 6890 N GC/5973 MSD, USA) with a DB-1701 column (30 m \times 0.25 mm, 1 μ m). All DBPs were identified and quantified using electron ionization under the selected ion monitoring (SIM) mode. Haloacetic acid (HAA) quantification followed a method adapted from EPA method 552.3 (USEPA, 2003). In brief, the pH of 3-mL samples were adjusted down to below 0.5, and 3 mL of MTBE (with 200 μ g L⁻¹ 1,2,3-trichloropropane as internal standard) was added. The samples were vortexed for 5 min, after which 2 mL of the MTBE extracts were transferred to a new vial and HAAs were converted to methyl esters by adding 2 mL of acidic methanol (10 vol%; 18 M H₂SO₄). The samples were then vortexed for 30 s and placed in a 50 °C water bath for 2 h. All HAAs were analyzed via gas chromatography coupled with electron capture detection (GC/ECD; Agilent 6890N, USA), wherein an Rxi-5 ms column (30 m × 0.25 mm,

 $0.25~\mu m$; Restek, Inc., Bellefonte, PA, USA) and N_2 carrier gas were employed. The GC oven program details are in Table S4. The DBP method quantification limits (MQL) and percent recovery are detailed in Text S1 and presented in Tables S5, S6, and S7.

3. Results and discussion

3.1. Property characterization of pyDOM extracted from grass and wood chars

The NPOC (panel A), TN (panel B), SUVA₂₅₄ (panel C), E₂/E₃ (panel D), EDC and EAC (panel E) values for all ten pyDOM samples from the oak wood and switchgrass chars as well as for the SRNOM are shown in Fig. 1. Similar to previous studies (Bostick et al., 2018; Hohner et al., 2019; Uchimiya et al., 2015; Xu et al., 2021), the NPOC values of pyDOM, regardless of the feedstock materials, were the highest for the lowest temperature chars (300 °C) and decreased with increasing pyrolysis temperature. The TN values of pyDOM followed a similar trend. We attribute both NPOC and TN trends to the decrease in water-soluble content of the wood and grass chars as the pyrolysis temperature increased. Specifically, as the charring temperature increased, chars became more apolar as shown in the decreasing H/C and O/C ratios and increasing double bond equivalence (DBE) values (Table S1). The SUVA₂₅₄ values of pyDOM decreased with increasing pyrolysis temperature regardless of feedstock materials, whereas the E2/E3 ratios increased, suggesting that pyDOM from higher temperature chars featured less aromaticity and lower molecular weights, which is consistent with previous studies (Wei et al., 2019; Wu et al., 2019; Xu et al., 2021). Moreover, pyDOM from low-temperature switchgrass chars (pyDOM $_{G300}$ vs. pyDOM $_{W300}$) exhibited higher NPOC and lower SUVA₂₅₄ values as compared to that from wood char, which could be attributed to the chemical structure differences in feedstock materials. Specifically, switchgrass contained higher content of polar, non-

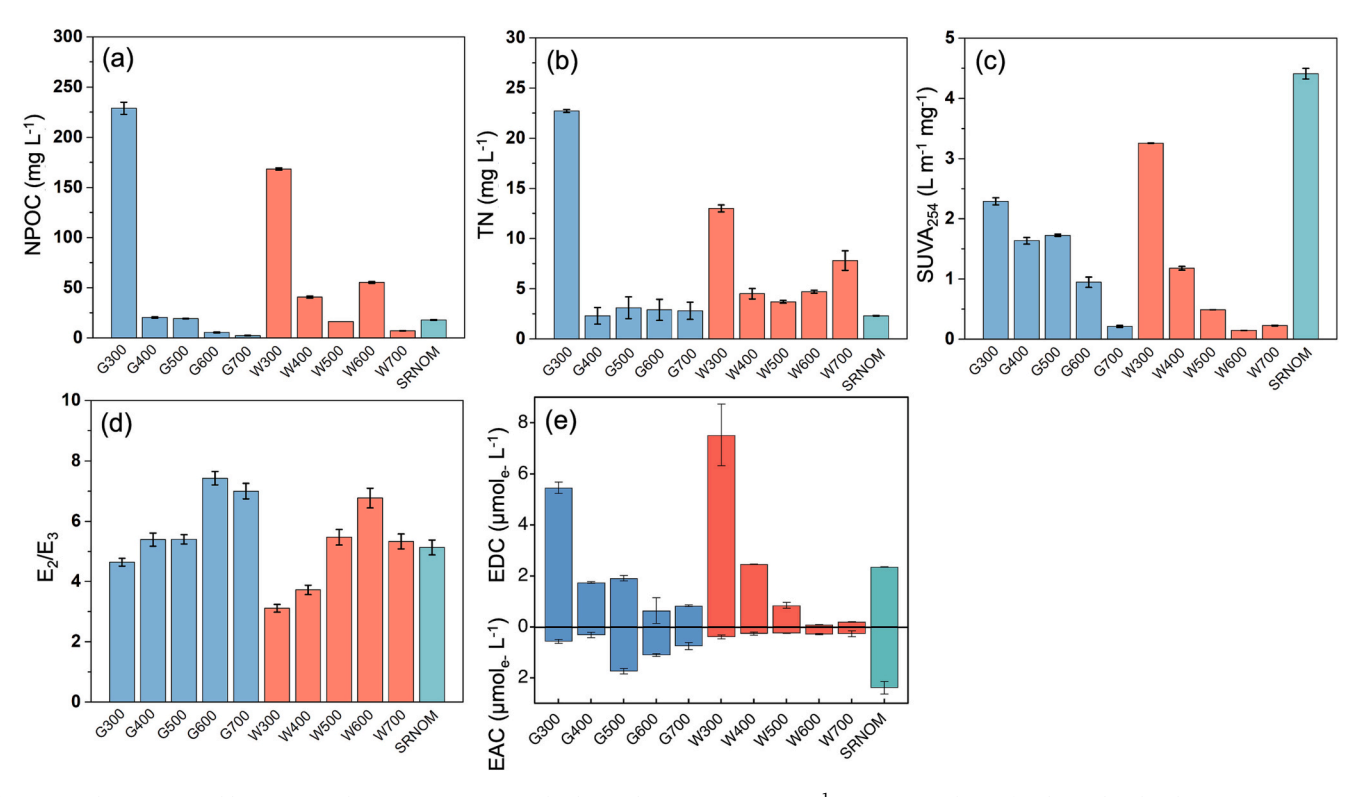


Fig. 1. (a) The non-purgeable organic carbon (NPOC) contents, (b) the total nitrogen (TN, mg L^{-1}), (c) measured specific ultraviolet absorbance (SUVA₂₅₄, L m⁻¹ mg⁻¹), (d) E_2/E_3 values, and (e) non-purgeable organic carbon (NPOC)-normalized EDC and EAC (mmol_e– g_c^{-1}) of pyDOM extracted from 10 chars as a function of the charring temperature (in °C) of chars prepared from grass (G) and wood (W) feedstock (20 g L^{-1}) as well as from reference SRNOM (50 mg L^{-1}). *** indicates that the obtained values were below the level of quantification limits. Error bars represent the standard deviation from experimental duplicates.

aromatic cellulose and hemicellulose contents as well as lower aromatic lignin contents compared to wood, which likely influenced the charderived pyDOM at low charring temperatures (Nimz et al., 1981; Xu et al., 2021; Zhao et al., 2012).

As expected, all pyDOM specimens were redox-active as shown in the EEC (mmol $_{\rm e-}$ g $_{\rm C}^{-1}$), calculated as the sum of EDC and EAC (Fig. 1E; Table S3). This study, for the first time, investigated the redox properties of pyDOM derived from field samples. Higher EDC values were observed for pyDOM from chars prepared at lower pyrolysis temperatures regardless of feedstock material, the values of which further decreased with increasing pyrolysis temperature. We attribute the observed trend to the decrease of electron-donating moieties, possibly phenols in pyDOM (Xu et al., 2021). The EAC of pyDOM derived from switchgrass char showed a maxima at 500 °C, whereas those derived from wood char showed minimum variation. It is possible that the cellulose/hemicellulose and lignin content were converted into C=O moieties during

pyrolysis, thereby contributing to the EAC of these pyDOM samples (Yang et al., 2007).

Analysis was performed on the possible contribution of two major redox-active transition metals that are mainly observed in the Earth's crust (Huang and Zhang, 2020) and were expected to be present, namely Fe and Mn. Both metals have a wide range of valence states (-4 to +4 for Fe and -3 to +7 for Mn), allowing their participation in a variety of redox reactions, which may ultimately influence DBP formation. Our results indicated that the overall EEC of all pyDOM samples indicated that the contribution of Fe to EEC was negligible (<5 %) (Table S2). However, the contribution of Mn became significant for pyDOM as pyrolysis temperature increased (i.e., pyDOM_{G400}, pyDOM_{G500}, pyDOM_{G600}, pyDOM_{G700}, pyDOM_{W600}) but remained negligible for those derived from low-temperature chars and majority of the wood chars (i.e., pyDOM_{G300}, pyDOM_{W300}, pyDOM_{W400}, pyDOM_{W500}, pyDOM_{W700}). We presume that redox-active organic moieties rather

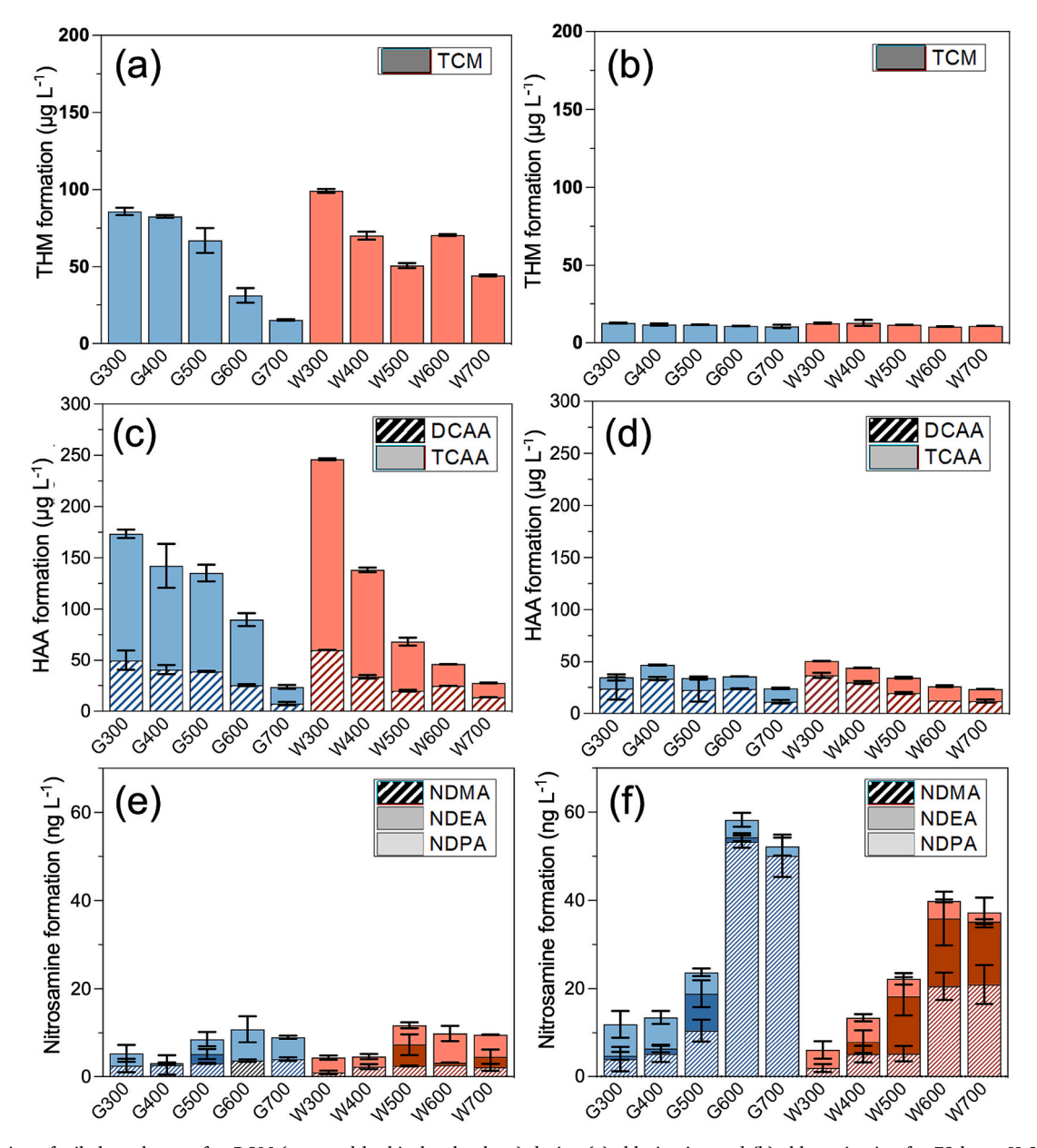


Fig. 2. Formation of trihalomethanes of pyDOM (prepared by biochar leachate) during (a) chlorination and (b) chloramination for 72 h at pH 8. Formation of haloacetic acids of pyDOM (prepared by biochar leachate) during (c) chlorination and (d) chloramination for 72 h at pH 8. Formation of *N*-nitrosamines of pyDOM (prepared by biochar leachate) during (e) chlorination and (f) chloramination for 72 h at pH 8. Error bars represent the standard deviation of experimental duplicates.

than metals were predominant in the EDC and EAC values of these pyDOM specimens. The role of metals in DBP formation is beyond the scope of this study.

3.2. Formation of THMs, HAAs, and N-nitrosamines during chlorination and chloramination

Our results from chlorination and chloramination suggest that chloroform (TCM) was the only detectable THM among the four THMs (Fig. 2a and b), whereas dichloroacetic acid (DCAA) and trichloroacetic acid (TCAA) were the only detectable HAAs among the nine HAAs (Fig. 2c and d). Three N-nitrosamines, namely N-nitrosodimethylamine (NDMA), N-nitrosodiethylamine (NDEA), and N-nitrosodi-n-propylamine (NDPA), of the seven N-nitrosamines investigated were observed in water samples containing either pyDOM following chlorination or chloramination (Fig. 2e and f). Blank controls without pyDOM (data not shown) did not show any THMs, HAAs, and N-nitrosamines, suggesting negligible DBP formation in the absence of pyDOM. As expected, the chlorinated samples exhibited higher formation of THM and HAA but lower N-nitrosamine formation as compared to their chloraminated counterparts. Closer inspection of Fig. 2 indicates that the speciation of HAA during disinfection was largely affected by the oxidant type (i.e., chlorine vs. chloramine). For instance, chlorination generated more TCAA than DCAA, whereas chloramination produced more DCAA than TCAA, which is in line with previous findings (Bougeard et al., 2010; Cowman and Singer, 1996; Sérodes et al., 2003). For the N-nitrosamines, this is the first study to observe the formation of NDEA and NDPA from pyDOM, whereas previous studies focused solely on NDMA (Chen et al., 2022; Chen et al., 2021; Wang et al., 2015b). In general, the pyrolysis temperature largely influenced N-nitrosamine speciation regardless of the feedstock materials, wherein the presence of NDEA and NDPA increased up to 11.4- and 2.9-fold, respectively, as pyrolysis temperature increased from 300 to 700 °C (Fig. 2e and f). A clear trend with pyrolysis temperature was observed following chlorination in water samples containing pyDOM, wherein HAA and THM formation decreased with increasing pyrolysis temperatures regardless of the feedstock materials. A similar trend was observed during chloramination, though at a lesser extent. By contrast, N-nitrosamine formation increased with pyrolysis temperature regardless of the feedstock materials or disinfectant type. As expected, the chloraminated samples showed higher N-nitrosamine formation as compared to the chlorinated ones (Gerecke and Sedlak, 2003; Selbes et al., 2013; Shah and Mitch, 2012).

We further performed correlation analyses on THM/HAA formation against the putative descriptor (i.e., SUVA254), and N-nitrosamine formation against the TN (Fig. S2). THM formation during chlorination showed good correlation with their SUVA₂₅₄ values (i.e., $R^2 = 0.79$), but poor correlation was observed under chloramination (i.e., $R^2 = 0.34$) (Fig. S2a and b). Similarly, HAA formation during chlorination correlated well with their SUVA $_{254}$ values (i.e., $R^2=0.97$), but poor correlation was found in chloramination (i.e., $R^2=0.42$) (Fig. S2c and d). Our observations are consistent with previous findings (Duirk and Valentine, 2006; Hua et al., 2015; Kanokkantapong et al., 2006; Tak and Vellanki, 2018). Specifically, the good correlation between THM/HAA and SUVA₂₅₄ following chlorination may be explained by the reaction between Cl2 and the organic precursors captured by SUVA254 in forming THM/HAA. For instance, previous studies suggest that the aromatic moieties (e.g., hydroxylated phenols) (Bond et al., 2012; Bougeard et al., 2010; Dickenson et al., 2008; He et al., 2018; Kanokkantapong et al., 2006; Tak and Vellanki, 2018) are responsible for the formation of THM/HAA in NOM. Similar types of precursors might present in pyDOM, contributing to HAA and THM formation during chlorination (Hua et al., 2015; Li et al., 2022). The observed speciation shifts in HAA, THM, and the *N*-nitrosamine formation following chloramination can be explained by the differences in the reactivity of disinfectants and reaction mechanisms. For instance, the higher formation of DCAA as compared to TCAA following chloramination may be contributed to

monochloramines being weaker oxidants as compared to chlorine with aromatic precursors (Brezonik and Arnold, 2022; Duirk and Valentine, 2006; Shah and Mitch, 2012), which may have hindered the attachment of a third halogen.

To a certain extent, our *N*-nitrosamine results can be explained by the N/C ratios—N-nitrosamine formation increased with pyrolysis temperature among the pyDOM specimens and correlated well with the N/C ratio (Table S3). However, for pyDOM samples with similar N/C ratios (i.e., $pyDOM_{W300}$ (0.077) versus $pyDOM_{W600}$ (0.085)), $pyDOM_{W600}$ showed a more than six-fold higher N-nitrosamine formation than pyDOM_{W300}, suggesting that N/C ratios alone cannot explain the observed trend for N-nitrosamine formation. This is supported by the poor correlation analysis on N-nitrosamine formation against TN (Fig. S2). It is likely that a subset of the N-containing organic precursors predominantly contributed to the formation of N-nitrosamines, the presence of which presumably increased with pyrolysis temperature (Knicker, 2007; Li et al., 2017; Liu et al., 2014; Selbes et al., 2013; Shah and Mitch, 2012; Torres-Rojas et al., 2020). For instance, the aliphatic amines (e.g., secondary, tertiary, and quaternary amines) or amine functional groups in biomolecules may be preserved in pyDOM after pyrolysis, which are known to be orders of magnitude more reactive with disinfectants than amide nitrogens (Shah and Mitch, 2012) and can thus contribute to the increased N-nitrosamine formation with increasing pyrolysis temperatures (Mitch and Sedlak, 2002; Piazzoli et al., 2018; Shah and Mitch, 2012; Wilczak et al., 2003). Although NDMA is the most frequently observed N-nitrosamines in previous studies (Mitch and Sedlak, 2002; Piazzoli et al., 2018; Shah and Mitch, 2012; Wilczak et al., 2003), we found a large amount of NDPA following chlorination regardless of feedstock materials. Although current water regulations predominantly focus on NDMA removal in water systems, our study suggests that other nitrogen-based DBPs, such as NDPA and NDEA, may also warrant attention.

3.3. Impacts of redox properties of pre- and post-fire field samples and their DBP formation

To evaluate the impact of wildfire on DBP formation, we performed both chlorination and chloramination experiments on pyDOM extracted from pre- (Pre_6, Pre_10) and post-fire (Post_6, Post_10) field samples. SRNOM was also included as a reference DOM. All samples underwent disinfection using the same procedure described in Section 2.5, the results of which are summarized in Fig. 3. Similar to the laboratoryderived pyDOM samples, the same DBP species were observed in the field samples, namely, TCM for THM (Fig. 3a and b), DCAA and TCAA for HAAs (Fig. 3c and d), and NDMA, NDEA, and NDPA for N-nitrosamines following chlorination or chloramination (Fig. 3e and f). As compared to the pre-fire samples, the post-fire samples exhibited decreased formations of THM (e.g., 63.9 ± 3.0 for Pre 6 to 46.0 ± 4.6 µg L^{-1} for Post 6; 46.4 \pm 1.6 for Pre 10 to 34.2 \pm 4.5 μ g L^{-1} for Post 10) and HAA (e.g., 186.5 ± 21.2 for Pre 6 to $116.3 \pm 19.3 \,\mu g \, L^{-1}$ for Post 6; 113.2 ± 7.0 for Pre 10 to $101.0 \pm 6.7~\mu g~L^{-1}$ for Post 10) under chlorination (Fig. 3a and c). A similar trend was observed under chloramination, though at a much lower extent. Higher N-nitrosamine formation was observed with the post-fire samples regardless of the disinfection scenario. Notably, the Post_6 fire samples showed 5.3-fold higher Nnitrosamine formation under chlorination as compared to the Post 10 fire samples (i.e., 1.4-fold increase), while minimal difference was observed between the two sites under chloramination (Fig. 3e and f). Despite the presence of NDMA, a significant amount of NDPA and NDEA formation were observed with both pyDOM and SRNOM, which has not been previously reported — of which NDEA and NDPA accounted for up to 73.5 % and 68.7 % (chlorination) and 16.8 % and 63.7 % (chloramination), respectively, of the total N-nitrosamine formation among all measured N-nitrosamines. At the same concentration of 3 mg_C L^{-1} , SRNOM showed up to 5.3- and 2.7-fold higher THM and HAA formation, respectively, as compared to pyDOM samples. By contrast, pyDOM from

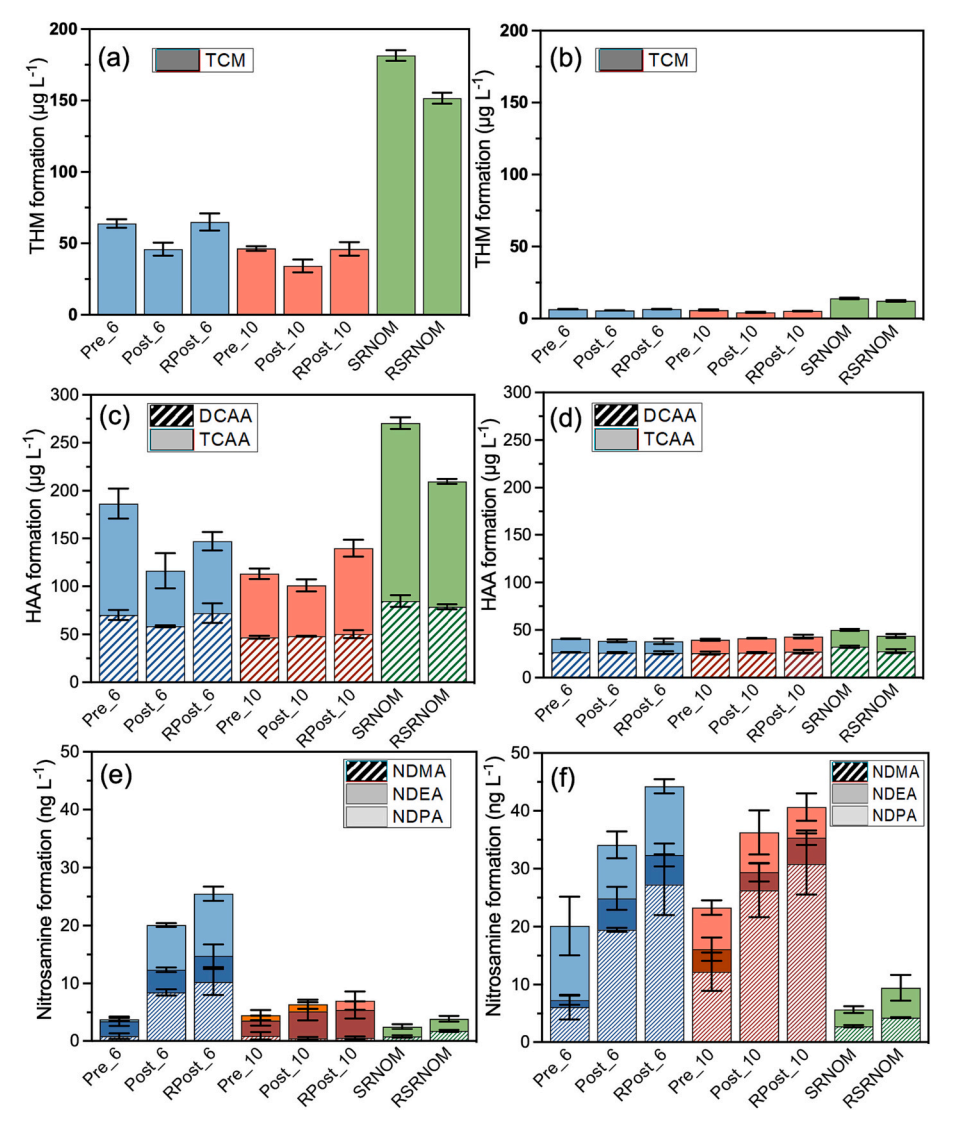


Fig. 3. Formation of trihalomethanes from pre- and post-fire soil samples and SRNOM as well as their reduced versions during (a) chlorination and (b) chloramination for 72 h at pH 8. Formation of haloacetic acids from pre- and post-fire soil samples and SRNOM as well as their reduced (R) versions during (c) chlorination and (d) chloramination for 72 h at pH 8. Formation of *N*-nitrosamines from pre- and post-fire soil samples and SRNOM as well as their reduced versions during (e) chlorination and (f) chloramination for 72 h at pH 8. Error bars represent the standard deviation of experimental duplicates.

the field samples exhibited up to 7.9-fold higher *N*-nitrosamine formation as compared to SRNOM. Additionally, SRNOM only showed NDMA and NDPA as the predominant *N*-nitrosamine species (Fig. 3).

The same THM, HAA, and N-nitrosamine species were observed between the laboratory and field samples. In addition, the lower THM and HAA formation as well as the higher N-nitrosamine formation in the post-fire samples under both disinfection scenarios are in line with our observations from the laboratory-derived pyDOM (Section 3.2). However, the impact of burning severity on DBP formation in field samples is much more complex. For instance, Site 6 exhibited a 5.3-fold higher Nnitrosamine formation than Site 10 (1.4-fold increase) under chlorination despite Site 6 having a lower burning severity as compared to Site 10 (Fig. 3e and f). We propose that these differences might also reflect variations in site conditions (e.g., differences in biomass and forest composition, the history of past fire incidents of the ecosystem) (Miesel et al., 2018). For instance, the lower portions of the forest floor layer (i. e., the more decomposed parts) likely contain some 'legacy' chars, which may already be present in this study's pre-fire samples. In addition, finer particles in the older char from previous fires may physically fragment over time. As such, the integrity of these 'legacy' chars and their subsequent influence on DBP formation may be maintained at lowseverity field locations as compared to high-severity field locations, as evinced by the initially high TCM and TCAA formation with Pre 6 as compared to Pre_10 (Fig. 3a and c). In addition, the laboratory-derived

samples showed decreasing SUVA $_{254}$ values as the pyrolysis temperatures increased, whereas the post-fire field samples presented higher SUVA $_{254}$ values than their pre-fire counterparts. Despite the higher N/C ratio (0.129) of SRNOM as compared to the pre-fire samples (N/C $_{\rm Pre_6}$: 0.122; N/C $_{\rm Pre_10}$: 0.092;), much lower *N*-nitrosamine formation was observed for SRNOM during both chlorination and chloramination (Fig. 3e and f).

To understand the effects of environmental redox conditions on pyDOM after wildfire and their subsequent influence on DBP formation, three pyDOM samples (i.e., Post_6, Post_10, and SRNOM) were chosen for electrochemical reduction treatment and the obtained samples were abbreviated as RPost_6, RPost_10, and RSRNOM, respectively, as detailed in Section 2.4.2. The NPOC-normalized EDC and EAC values for these samples before and after reduction are tabulated in Table S3. No significant changes in NPOC or TN concentrations were observed before and after electrochemical reduction. As expected, all three samples showed an increase in EDC and a decrease in EAC after electrochemical reduction. Post_6 and Post_10 exhibited a decrease of 1.56 and 0.50 $mmol_{e-}$ g_C^{-1} in EAC and an increase of 0.16 and 0.22 $mmol_{e-}$ g_C^{-1} in EDC, respectively. By contrast, the increase in EDC and decrease in EAC were comparable for SRNOM, which has also been observed with DOM (Walpen et al., 2018). Following chlorination, both reduced post-fire samples (RPost 6, RPost 10) exhibited higher THM, HAA, and N-nitrosamine formation as compared to their pre-reduced counterparts (Fig. 3a, c, e). In comparison, chloramination resulted in similar, yet lower, THM and HAA formation (Fig. 3b, d) but higher *N*-nitrosamine formation (Fig. 3f). The smaller increase in EDC as compared to the decrease in EAC for all field samples suggests that only a portion of the redox moieties responsible for EAC can be reversibly converted to EDC moieties during the electrochemical reduction treatment. By contrast, the comparable increase in EDC and decrease in EAC for SRNOM following electrochemical reduction suggests the presence of largely reversible redox moieties in SRNOM (Cao et al., 2023; Xu et al., 2021).

The higher THM, HAA formation with RPost_6 and RPost_10 can be partly explained by their higher abundance of phenolic moieties after electrochemical reduction as reflected by the larger EDC values (Table S3). These results are in line with previous studies that also observed higher THM, HAA formation with increased phenolic contents (Bond et al., 2012; Cordero et al., 2020; Dickenson et al., 2008; Ge et al., 2013). The lower THM, HAA formation with RSRNOM could be possibly ascribed to a lower aromaticity as reflected by its lower SUVA₂₅₄ values following electrochemical reduction (3.31 to 2.98 L m⁻¹ mg⁻¹ in Table S3). We observed increase in N-nitrosamines formation for RPost 6, RPost 10, and RSRNOM. This can be explained by the formation of nitrogen-based DBP precursors (e.g., aliphatic amines, amine functional groups) or intermediates (e.g., nitro or nitroso compounds) during the electrochemical reduction due to bond dissociation as reflected by the changes in their E2/E3 values (e.g., Post_6 (7.79) vs. RPost_6 (10.52)) (Aeschbacher et al., 2012a; Walpen et al., 2018; Wirtanen et al., 2020; Yang et al., 2016).

4. Conclusions

Our findings of increased nitrogen-based DBP formation, especially those unregulated N-nitrosamines such as NDMA, NDEA, and NDPA, in waters containing pyDOM from higher temperature chars and post-fire samples raise concerns for drinking water safety and DBP mitigation measures. In particular, the water quality for communities that rely on the forest watersheds can be significantly affected by the release of pyDOM during the post-fire recovery effort. While the USEPA has yet to mandate any comprehensive regulations for N-nitrosamines, the formation of nitrogen-based DBPs in water systems poses particular concerns due to their higher cyto- and genotoxicity as compared to regulated carbon-based DBPs (i.e., THMs, HAAs) (Goslan et al., 2009; Muellner et al., 2007; Plewa et al., 2004). Moreover, the majority of past studies have focused on the formation of NDMA given its prevalence following disinfection processes (Mitch and Schreiber, 2008; Schreiber and Mitch, 2005). For instance, previous studies investigated chlorinated recreational waters using EPA Method 521 for N-nitrosamines, from which NDMA only accounted for an average of 13 % of the Nnitrosamine pool (Kulshrestha et al., 2010; Shah and Mitch, 2012). By contrast, this is the first study to report NDEA and NDPA formation at levels that are as high (or sometimes higher) than NDMA under both chlorination and chloramination from both the laboratory and field samples. Our findings that NDEA and NDPA, which are currently on the USEPA second Unregulated Contaminant Monitoring Rule (UCMR 2) (USEPA, 2008), are present at significant levels support the need to broaden the current DBP monitoring and mitigation efforts to include other N-DBPs. This aspect is particularly important for small water systems that dependent upon forest watersheds and are prone to wildfires. Furthermore, our study demonstrated that pyDOM from both laboratory-derived char and field samples produced up to 5 ng L⁻¹ NDMA at $3 \text{ mg}_{\text{C}} \text{ L}^{-1}$, which is above the USEPA screening level of 0.11 ng L^{-1} in tap water (USEPA, 2017) and in the same range as NDMA observed in water samples impacted by algal cell- and algal organic matter (Li et al., 2020; Tsai et al., 2019; Zhou et al., 2015). All of these suggest that pyDOM might be an important N source for nitrogen-based DBP formation. Formation of other nitrogen-based DBPs such as haloacetonitriles and halonitromethanes warrants further investigation.

Lastly, our findings indicate that electrochemical reduction of

pyDOM from the post-fire samples resulted in increased THM, HAA, and N-nitrosamine formation by up to 41.4 % under chlorination and 29.6 % under chloramination. These results suggest that the reducing environmental conditions might help preserve these DBP precursors, which can subsequently participate long-range transport due to their smaller molecular weights and higher polarities or interact with fine particulates from 'legacy' chars in fire-prone ecosystems and thus undergo particulate-facilitated transport. The stability and aging effects of pyDOM in the environment and their subsequent impact on DBP formation for communities that are susceptible to wildfires warrants further investigation.

CRediT authorship contribution statement

Zhao Li: Data curation, Formal analysis, Methodology, Writing – original draft. **Pamela Rose V. Samonte:** Formal analysis, Writing – review & editing. **Han Cao:** Data curation, Formal analysis, Writing – review & editing. **Jessica R. Miesel:** Formal analysis, Writing – review & editing. **Wenqing Xu:** Project administration, Formal analysis, Supervision, Writing – review & editing.

Declaration of competing interest

The authors declare that they have no known competing financial interests or personal relationships that could have appeared to influence the work reported in this paper.

Data availability

Data will be made available on request.

Acknowledgments

W.X. and H.C. acknowledge the U.S. National Science Foundation CAREER award (CBET-1752220) for the financial support. W.X also acknowledges support by the U.S. Department of Defense through the Strategic Environmental Research and Development Program (SERDP ER19-1239). J.M. acknowledges support from McIntire-Stennis project MICL-06033. J.M. would like to thank the USDA Forest Service Fire Behavior Assessment Team for assistance in obtaining the field samples.

Appendix A. Supplementary data

Supplementary data to this article can be found online at https://doi.org/10.1016/j.scitotenv.2023.165496.

References

Abiven, S., Hengartner, P., Schneider, M.P.W., Singh, N., Schmidt, M.W.I., 2011.

Pyrogenic carbon soluble fraction is larger and more aromatic in aged charcoal than in fresh charcoal. Soil Biol. Biochem. 43 (7), 1615–1617.

Aeschbacher, M., Sander, M., Schwarzenbach, R.P., 2010. Novel electrochemical approach to assess the redox properties of humic substances. Environ. Sci. Technol. 44 (1), 87–93.

Aeschbacher, M., Brunner, S.H., Schwarzenbach, R.P., Sander, M., 2012a. Assessing the effect of humic acid redox state on organic pollutant sorption by combined electrochemical reduction and sorption experiments. Environ. Sci. Technol. 46 (7), 3882–3890.

Aeschbacher, M., Graf, C., Schwarzenbach, R.P., Sander, M., 2012b. Antioxidant properties of humic substances. Environ. Sci. Technol. 46 (9), 4916–4925.

Association, A.P.H, Association, A.W.W, Federation, W.P.C., Federation, W.E., 1915.

Standard Methods for the Examination of Water and Wastewater. American Public Health Association.

Bladon, K.D., Emelko, M.B., Silins, U., Stone, M., 2014. Wildfire and the Future of Water Supply. ACS Publications.

Bond, T., Huang, J., Templeton, M.R., Graham, N., 2011. Occurrence and control of nitrogenous disinfection by-products in drinking water – a review. Water Res. 45 (15), 4341–4354.

Bond, T., Goslan, E.H., Parsons, S.A., Jefferson, B., 2012. A critical review of trihalomethane and haloacetic acid formation from natural organic matter surrogates. Environ. Technol. Rev. 1 (1), 93–113.

- Bostick, K.W., Zimmerman, A.R., Wozniak, A., Mitra, S., Hatcher, P.G., 2018. Production and composition of pyrogenic dissolved organic matter from a logical series of laboratory-generated chars. Front. Earth Sci. 6, 43.
- Bougeard, C.M.M., Goslan, E.H., Jefferson, B., Parsons, S.A., 2010. Comparison of the disinfection by-product formation potential of treated waters exposed to chlorine and monochloramine. Water Res. 44 (3), 729–740.
- Brezonik, P.L., Arnold, W.A., 2022. In: Brezonik, P.L., Arnold, W.A. (Eds.), Chapter 15: Chemistry of Chlorine and Other Oxidants/Disinfectants. Oxford University Press.
- Cannon, S.H., DeGraff, J., 2009. Landslides–disaster Risk Reduction. Springer, pp. 177–190.
- Chen, H., Tsai, K.-P., Liu, Y., Tolić, N., Burton, S.D., Chu, R., Karanfil, T., Chow, A.T., 2021. Characterization of dissolved organic matter from wildfire-induced Microcystis aeruginosa blooms controlled by copper sulfate as disinfection byproduct precursors using APPI(-) and ESI(-) FT-ICR MS. Water Res. 189, 116640.
- Cao, H., Pavitt, A.S., Hudson, J.M., Tratnyek, P.G., Xu, W., 2023. Electron exchange capacity of pyrogenic dissolved organic matter (pyDOM): complementarity of square-wave voltammetry in DMSO and mediated chronoamperometry in water. Environ. Sci.: Process. Impacts 25 (4), 767–780.
- Chen, H., Ersan, M.S., Tolić, N., Chu, R.K., Karanfil, T., Chow, A.T., 2022. Chemical characterization of dissolved organic matter as disinfection byproduct precursors by UV/fluorescence and ESI FT-ICR MS after smoldering combustion of leaf needles and woody trunks of pine (Pinus jeffreyi). Water Res. 209, 117962.
- Cordero, J.A., He, K., Okuta, E., Echigo, S., Itoh, S., 2020. Effect of biodegradation on haloacetic acid formation potentials of anthropogenic compounds during chlorination. Environ. Sci. Pollut. Res. 27 (15), 18117–18128.
- Cowman, G.A., Singer, P.C., 1996. Effect of bromide ion on haloacetic acid speciation resulting from chlorination and chloramination of aquatic humic substances. Environ. Sci. Technol. 30 (1), 16–24.
- DeMarini, D.M., 2020. A review on the 40th anniversary of the first regulation of drinking water disinfection by-products. Environ. Mol. Mutagen. 61 (6), 588–601.
- Dickenson, E.R.V., Summers, R.S., Croué, J.-P., Gallard, H., 2008. Haloacetic acid and trihalomethane formation from the chlorination and bromination of aliphatic β-dicarbonyl acid model compounds. Environ. Sci. Technol. 42 (9), 3226–3233.
- Duirk, S.E., Valentine, R.L., 2006. Modeling dichloroacetic acid formation from the reaction of monochloramine with natural organic matter. Water Res. 40 (14), 2667–2674
- Eidenshink, J., Schwind, B., Brewer, K., Zhu, Z.-L., Quayle, B., Howard, S., 2007. A project for monitoring trends in burn severity. Fire Ecol. 3 (1), 3–21.
- Emelko, M.B., Silins, U., Bladon, K.D., Stone, M., 2011. Implications of land disturbance on drinking water treatability in a changing climate: demonstrating the need for "source water supply and protection" strategies. Water Res. 45 (2), 461–472.
- Fu, H., Liu, H., Mao, J., Chu, W., Li, Q., Alvarez, P.J., Qu, X., Zhu, D., 2016. Photochemistry of dissolved black carbon released from biochar: reactive oxygen species generation and phototransformation. Environ. Sci. Technol. 50 (3), 1218–1226.
- Furman, C.S., Margerum, D.W., 1998. Mechanism of chlorine dioxide and chlorate ion formation from the reaction of hypobromous acid and chlorite ion. Inorg. Chem. 37 (17), 4321–4327.
- Ge, F., Tang, F., Xu, Y., Xiao, Y., 2013. Formation characteristics of haloacetic acids from phenols in drinking water chlorination. Water Supply 14 (1), 142–149.
- phenois in artiking water chromation. Water Supply 14 (1), 142–149. Gerecke, A.C., Sedlak, D.L., 2003. Precursors of N-nitrosodimethylamine in natural waters. Environ. Sci. Technol. 37 (7), 1331–1336.
- Goslan, E.H., Krasner, S.W., Bower, M., Rocks, S.A., Holmes, P., Levy, L.S., Parsons, S.A., 2009. A comparison of disinfection by-products found in chlorinated and chloraminated drinking waters in Scotland. Water Res. 43 (18), 4698–4706.
- He, K., Okuta, E., Cordero, J.A., Echigo, S., Asada, Y., Itoh, S., 2018. Formation of chlorinated haloacetic acids by chlorination of low molecular weight compounds listed on pollutant release and transfer registers (PRTRs). J. Hazard. Mater. 351, 98–107.
- Hohner, A.K., Cawley, K., Oropeza, J., Summers, R.S., Rosario-Ortiz, F.L., 2016. Drinking water treatment response following a Colorado wildfire. Water Res. 105, 187-198.
- water treatment response following a Colorado wildfire. Water Res. 105, 187–198. Hohner, A.K., Rhoades, C.C., Wilkerson, P., Rosario-Ortiz, F.L., 2019. Wildfires alter forest watersheds and threaten drinking water quality. Acc. Chem. Res. 52 (5), 1234–1244.
- Hua, G., Reckhow, D.A., Abusallout, I., 2015. Correlation between SUVA and DBP formation during chlorination and chloramination of NOM fractions from different sources. Chemosphere 130, 82–89.
- Huang, J., Zhang, H., 2020. Redox reactions of iron and manganese oxides in complex systems. Front. Environ. Sci. Eng. 14 (5), 76.
- Jaffé, R., Ding, Y., Niggemann, J., Vähätalo, A.V., Stubbins, A., Spencer, R.G.M., Campbell, J., Dittmar, T., 2013. Global charcoal mobilization from soils via dissolution and riverine transport to the oceans. Science 340 (6130), 345–347.
- Kanokkantapong, V., Marhaba, T.F., Pavasant, P., Panyapinyophol, B., 2006. Characterization of haloacetic acid precursors in source water. J. Environ. Manag. 80 (3), 214–221.
- Klüpfel, L., Piepenbrock, A., Kappler, A., Sander, M., 2014. Humic substances as fully regenerable electron acceptors in recurrently anoxic environments. Nat. Geosci. 7 (3), 195–200.
- Knicker, H.E., 2007. How does fire affect the nature and stability of soil organic nitrogen and carbon? A review. Biogeochemistry 85, 91–118.
- Krasner, S.W., 2009. The formation and control of emerging disinfection by-products of health concern. Philos. Trans. R. Soc. London A Math. Phys. Eng. Sci. 367 (1904), 4077–4095.
- Kulshrestha, P., McKinstry, K.C., Fernandez, B.O., Feelisch, M., Mitch, W.A., 2010.
 Application of an optimized total N-nitrosamine (TONO) assay to pools: placing N-

- nitrosodimethylamine (NDMA) determinations into perspective. Environ. Sci. Technol. 44 (9), 3369–3375.
- Lee, H.-S., Kim, Y., Kim, J., Shin, H.-S., 2022. Quantitative and qualitative characteristics of dissolved organic matter derived from biochar depending on the modification method and biochar type. J. Water Process Eng. 46, 102569.
- Li, Z., Chen, T., Cui, F., Xie, Y., Xu, W., 2017. Impact of chitosan and polyacrylamide on formation of carbonaceous and nitrogenous disinfection by-products. Chemosphere 178, 26–33.
- Li, X., Rao, N.R.H., Linge, K.L., Joll, C.A., Khan, S., Henderson, R.K., 2020. Formation of algal-derived nitrogenous disinfection by-products during chlorination and chloramination. Water Res. 183, 116047.
- Li, L.-P., Liu, Y.-H., Ren, D., Wang, J.-J., 2022. Characteristics and chlorine reactivity of biochar-derived dissolved organic matter: effects of feedstock type and pyrolysis temperature. Water Res. 211, 118044.
- Liu, Y.D., Selbes, M., Zeng, C., Zhong, R., Karanfil, T., 2014. Formation mechanism of NDMA from ranitidine, trimethylamine, and other tertiary amines during chloramination: a computational study. Environ. Sci. Technol. 48 (15), 8653–8663.
- Liu, C., Wang, H., Li, P., Xian, Q., Tang, X., 2019. Biochar's impact on dissolved organic matter (DOM) export from a cropland soil during natural rainfalls. Sci. Total Environ. 650, 1988–1995.
- Maestrini, B., Alvey, E.C., Hurteau, M.D., Safford, H., Miesel, J.R., 2017. Fire severity alters the distribution of pyrogenic carbon stocks across ecosystem pools in a Californian mixed-conifer forest. J. Geophys. Res. Biogeosci. 122 (9), 2338–2355.
- Major, J., Lehmann, J., Rondon, M., Goodale, C., 2010. Fate of soil-applied black carbon: downward migration, leaching and soil respiration. Glob. Chang. Biol. 16 (4), 1366–1379
- Miesel, J., Reiner, A., Ewell, C., Maestrini, B., Dickinson, M., 2018. Quantifying changes in total and pyrogenic carbon stocks across fire severity gradients using active wildfire incidents. Front. Earth Sci. 6.
- Mitch, W.A., 2009. Occurrence and Formation of Nitrogenous Disinfection By-products. Water Research Foundation.
- Mitch, W.A., Schreiber, I.M., 2008. Degradation of tertiary alkylamines during chlorination/chloramination: implications for formation of aldehydes, nitriles, halonitroalkanes, and nitrosamines. Environ. Sci. Technol. 42 (13), 4811–4817.
- Mitch, W.A., Sedlak, D.L., 2002. Formation of N-nitrosodimethylamine (NDMA) from dimethylamine during chlorination. Environ. Sci. Technol. 36 (4), 588–595.
- Muellner, M.G., Wagner, E.D., McCalla, K., Richardson, S.D., Woo, Y.-T., Plewa, M.J., 2007. Haloacetonitriles vs. regulated haloacetic acids: are nitrogen-containing DBPs more toxic? Environ. Sci. Technol. 41 (2), 645–651.
- NAE, 2019. National Academy of Engineering Grand Challenge: Provide Access to Clean
- Nimz, H.H.H., Robert, D., Faix, O., Nemr, M.T.M., 1981. Carbon-13 NMR spectra of Lignins, 8. In: Structural Differences between Lignins of Hardwoods, Softwoods, Grasses and Compression Wood.
- Olivares, C.I., Uzun, H., Erdem, C.U., Zhang, W., Trettin, C., Liu, Y., Burton, S.D., Robinson, E.W., Karanfil, T., Chow, A.T., 2021. Increased organohalogen diversity after disinfection of water from a prescribed burned watershed. ACS ES&T Water 1 (5) 1274–1282
- Pals, J.A., Ang, J.K., Wagner, E.D., Plewa, M.J., 2011. Biological mechanism for the toxicity of haloacetic acid drinking water disinfection byproducts. Environ. Sci. Technol. 45 (13), 5791–5797.
- Pandian, A.M.K., Rajamehala, M., Singh, M.V.P., Sarojini, G., Rajamohan, N., 2022. Potential risks and approaches to reduce the toxicity of disinfection by-product – a review. Sci. Total Environ. 822, 153323.
- Piazzoli, A., Breider, F., Aquillon, C.G., Antonelli, M., von Gunten, U., 2018. Specific and total N-nitrosamines formation potentials of nitrogenous micropollutants during chloramination. Water Res. 135, 311–321.
- Plewa, M.J., Wagner, E.D., Jazwierska, P., Richardson, S.D., Chen, P.H., McKague, A.B., 2004. Halonitromethane drinking water disinfection byproducts: chemical characterization and mammalian cell cytotoxicity and genotoxicity. Environ. Sci. Technol. 38 (1), 62–68.
- Plewa, M.J., Wagner, E.D., Muellner, M.G., Hsu, K.-M., Richardson, S.D., 2008. Disinfection By-Products in Drinking Water. American Chemical Society, pp. 36–50.
- Qu, X., Fu, H., Mao, J., Ran, Y., Zhang, D., Zhu, D., 2016. Chemical and structural properties of dissolved black carbon released from biochars. Carbon 96, 759–767.
- Reich, P.B., Peterson, D.W., Wedin, D.A., Wrage, K., 2001. Fire and vegetation effects on productivity and nitrogen cycling across a forest–grassland continuum. Ecology 82 (6), 1703–1719.
- Revchuk, A.D., Suffet, I., 2014. Effect of wildfires on physicochemical changes of watershed dissolved organic matter. Water Environ. Res. 86 (4), 372–381.
- Rhoades, C.C., Nunes, J.P., Silins, U., Doerr, S.H., 2019. The influence of wildfire on water quality and watershed processes: new insights and remaining challenges. Int. J. Wildland Fire 28 (10), 721–725.
- Richardson, S.D., Ternes, T.A., 2014. Water analysis: emerging contaminants and current issues. Anal. Chem. 86 (6), 2813–2848.
- Richardson, S.D., Plewa, M.J., Wagner, E.D., Schoeny, R., DeMarini, D.M., 2007.
 Occurrence, genotoxicity, and carcinogenicity of regulated and emerging disinfection by-products in drinking water: a review and roadmap for research.
 Mutat. Res. Rev. Mutat. Res. 636 (1–3), 178–242.
- Samonte, P.R.V., Li, Z., Mao, J., Chaplin, B.P., Xu, W., 2022. Pyrogenic carbon-promoted haloacetic acid decarboxylation to trihalomethanes in drinking water. Water Res. 210, 117988.
- Santín, C., Doerr, S.H., Merino, A., Bucheli, T.D., Bryant, R., Ascough, P., Gao, X., Masiello, C.A., 2017. Carbon sequestration potential and physicochemical properties differ between wildfire charcoals and slow-pyrolysis biochars. Sci. Rep. 7 (1), 11233.

- Schreiber, I.M., Mitch, W.A., 2005. Influence of the order of reagent addition on NDMA formation during chloramination. Environ. Sci. Technol. 39 (10), 3811–3818.
- Selbes, M., Kim, D., Ates, N., Karanfil, T., 2013. The roles of tertiary amine structure, background organic matter and chloramine species on NDMA formation. Water Res. 47 (2), 945–953.
- Sérodes, J.B., Rodriguez, M.J., Li, H., Bouchard, C., 2003. Occurrence of THMs and HAAs in experimental chlorinated waters of the Quebec City area (Canada). Chemosphere 51 (4), 253–263.
- Shah, A.D., Mitch, W.A., 2012. Halonitroalkanes, halonitriles, haloamides, and N-nitrosamines: a critical review of nitrogenous disinfection byproduct formation pathways. Environ. Sci. Technol. 46 (1), 119–131.
- Smith, H.G., Sheridan, G.J., Lane, P.N., Nyman, P., Haydon, S., 2011. Wildfire effects on water quality in forest catchments: a review with implications for water supply. J. Hydrol. 396 (1–2), 170–192.
- Song, F., Li, T., Shi, Q., Guo, F., Bai, Y., Wu, F., Xing, B., 2021. Novel insights into the molecular-level mechanism linking the chemical diversity and copper binding heterogeneity of biochar-derived dissolved black carbon and dissolved organic matter. Environ. Sci. Technol. 55 (17), 11624–11636.
- Sun, Y., Xiong, X., He, M., Xu, Z., Hou, D., Zhang, W., Ok, Y.S., Rinklebe, J., Wang, L., Tsang, D.C.W., 2021. Roles of biochar-derived dissolved organic matter in soil amendment and environmental remediation: a critical review. Chem. Eng. J. 424, 130387.
- Tak, S., Vellanki, B.P., 2018. Natural organic matter as precursor to disinfection byproducts and its removal using conventional and advanced processes: state of the art review. J. Water Health 16 (5), 681–703.
- Torres-Rojas, D., Hestrin, R., Solomon, D., Gillespie, A.W., Dynes, J.J., Regier, T.Z., Lehmann, J., 2020. Nitrogen speciation and transformations in fire-derived organic matter. Geochim. Cosmochim. Acta 276, 170–185.
- Tsai, K.-P., Uzun, H., Chen, H., Karanfil, T., Chow, A.T., 2019. Control wildfire-induced Microcystis aeruginosa blooms by copper sulfate: trade-offs between reducing algal organic matter and promoting disinfection byproduct formation. Water Res. 158, 227–236.
- Uchimiya, M., Hiradate, S., Antal, M., 2015. Influence of carbonization methods on the aromaticity of pyrogenic dissolved organic carbon. Energy Fuel 29, 2503–2513.
- USEPA, USEPA (Eds.), 1995. Methods for the Determination of Organic Compounds in Drinking Water: Supplement 3.
- USEPA, 2003. Method 552.3: Determination of Haloacetic Acids and Dalapon in Drinking Water by Liquid-liquid Microextraction, Derivatization, and Gas Chromatography With Electron Capture Detection, Revision 1.0. U.S. EPA, Washington, D.C.
- USEPA, USEPA (Eds.), 2004. Determination of Nitrosamines in Drinking Water by Solid Phase Extraction and Capillary Column Gas Chromatography With Large Volume Injection and Chemical Ionization Tandem Mass Spectrometry (MS/MS). USEPA, Cincinnati. OH.
- USEPA, 2006. Stage 1 and Stage 2 Disinfectants and Disinfection Byproducts Rules.
- USEPA, 2008. Second Unregulated Contaminant Monitoring Rule.
 USEPA, USEPA (Eds.), 2017. Technical Fact Sheet N-Nitroso-dimethylamine (NDMA).
 USEPA, 2023. National Primary Drinking Water Regulations.
- Walpen, N., Schroth, M.H., Sander, M., 2016. Quantification of phenolic antioxidant moieties in dissolved organic matter by flow-injection analysis with electrochemical detection. Environ. Sci. Technol. 50 (12), 6423–6432.
- Walpen, N., Getzinger, G.J., Schroth, M.H., Sander, M., 2018. Electron-donating phenolic and electron-accepting quinone moieties in peat dissolved organic matter: quantities and redox transformations in the context of peat biogeochemistry. Environ. Sci. Technol. 52 (9), 5236–5245.
- Wang, J.-J., Dahlgren, R.A., Chow, A.T., 2015a. Controlled burning of forest detritus altering spectroscopic characteristics and chlorine reactivity of dissolved organic

- matter: effects of temperature and oxygen availability. Environ. Sci. Technol. 49 (24), 14019-14027.
- Wang, J.J., Dahlgren, R.A., Erşan, M.S., Karanfil, T., Chow, A.T., 2015b. Wildfire altering terrestrial precursors of disinfection byproducts in forest detritus. Environ. Sci. Technol. 49 (10), 5921–5929.
- Wang, J.-J., Dahlgren, R.A., Erşan, M.S., Karanfil, T., Chow, A.T., 2016. Temporal variations of disinfection byproduct precursors in wildfire detritus. Water Res. 99, 66–73.
- Wang, M., Liu, J., Peng, L., Tian, S., Yang, C., Xu, G., Wang, D., Jiang, T., 2021.
 Estimation of the biogeochemical reactivities of dissolved organic matter from modified biochars using color. Sci. Total Environ. 790, 147974.
- Wang, R., Zhou, J., Qu, G., Wang, T., Jia, H., Zhu, L., 2023. Formation of emerging disinfection byproducts from agricultural biomass-derived DOM: overlooked health risk source. Water Res. 229, 119482.
- Wei, S., Zhu, M., Fan, X., Song, J., Peng, P.A., Li, K., Jia, W., Song, H., 2019. Influence of pyrolysis temperature and feedstock on carbon fractions of biochar produced from pyrolysis of rice straw, pine wood, pig manure and sewage sludge. Chemosphere 218, 624–631.
- Wilczak, A., Assadi-Rad, A., Lai, H.H., Hoover, L.L., Smith, J.F., Berger, R., Rodigari, F., Beland, J.W., Lazzelle, L.J., Kincannon, E.G., Baker, H., Heaney, C.T., 2003. Formation of NDMA in chloraminated water coagulated with DADMAC cationic polymer. J. AWWA 95 (9), 94–106.
- Wirtanen, T., Rodrigo, E., Waldvogel, S.R., 2020. Recent advances in the electrochemical reduction of substrates involving N-O bonds. Adv. Synth. Catal. 362 (11), 2088–2101
- Writer, J.H., Hohner, A., Oropeza, J., Schmidt, A., Cawley, K.M., Rosario-Ortiz, F.L., 2014. Water treatment implications after the High Park Wildfire, Colorado. J. AWWA 106 (4), E189–E199.
- Wu, H., Qi, Y., Dong, L., Zhao, X., Liu, H., 2019. Revealing the impact of pyrolysis temperature on dissolved organic matter released from the biochar prepared from Typha orientalis. Chemosphere 228, 264–270.
- Xu, W., Walpen, N., Keiluweit, M., Kleber, M., Sander, M., 2021. Redox properties of pyrogenic dissolved organic matter (pyDOM) from biomass-derived chars. Environ. Sci. Technol. 55 (16), 11434–11444.
- Yang, H., Yan, R., Chen, H., Lee, D.H., Zheng, C., 2007. Characteristics of hemicellulose, cellulose and lignin pyrolysis. Fuel 86 (12–13), 1781–1788.
- Yang, Z., Kappler, A., Jiang, J., 2016. Reducing capacities and distribution of redoxactive functional groups in low molecular weight fractions of humic acids. Environ. Sci. Technol. 50 (22), 12105–12113.
- Yang, H., Ye, S., Wang, H., Zhou, C., Xiong, T., Deng, Y., Fu, Q., Zeng, G., Zeng, Z., Tan, X., 2022. Insight into disinfection byproduct formation potential of aged biochar and its effects during chlorination. J. Environ. Manag. 317, 115437.
- Zhang, B., Zhou, S., Zhou, L., Wen, J., Yuan, Y., 2019. Pyrolysis temperature-dependent electron transfer capacities of dissolved organic matters derived from wheat straw biochar. Sci. Total Environ. 696, 133895.
- Zhao, X., Zhang, L., Liu, D., 2012. Biomass recalcitrance. Part I: the chemical compositions and physical structures affecting the enzymatic hydrolysis of lignocellulose. Biofuels Bioprod. Biorefin. 6 (4), 465–482.
- Zheng, X., Liu, Y., Fu, H., Qu, X., Yan, M., Zhang, S., Zhu, D., 2019. Comparing electron donating/accepting capacities (EDC/EAC) between crop residue-derived dissolved black carbon and standard humic substances. Sci. Total Environ. 673, 29–35.
- Zhou, S., Zhu, S., Shao, Y., Gao, N., 2015. Characteristics of C-, N-DBPs formation from algal organic matter: role of molecular weight fractions and impacts of preozonation. Water Res. 72, 381–390.